International Journal of GEOMATE, Aug., 2022, Vol.23, Issue 96, pp.171-178
ISSN: 2186-2982 (P), 2186-2990 (O), Japan, DOI: https://doi.org/10.21660/2022.96.j2261
Geotechnique, Construction Materials and Environment

IDENTIFICATION OF TSUNAMI DEPOSIT AT MEULABOH, ACEH (INDONESIA) USING GROUND PENETRATING RADAR (GPR)

*Muhammad Syukri[1], Sabrian Tri Anda[2], Muksin Umar[3], Ella Meilianda[3], and Rosli Saad[4], Zul Fadhli[5] and Rini Safitri[1]

[1]Department of Physics, Faculty of Sciences, Syiah Kuala University, Banda Aceh, Indonesia.
[2]Physics Department, Engineering Faculty, Universitas Samudra, Indonesia.
[3]Tsunami and Disasters Mitigation Research Center (TDMRC), Syiah Kuala University, Indonesia.
[4]School of Physics, Universiti Sains Malaysia, 11800 Penang, Malaysia
[5]Department of Engineering Geophysics, Engineering Faculty, Syiah Kuala University, Indonesia.

*Corresponding Author, Received: 05 July 2021, Revised: 18 May 2022, Accepted: 12 June 2022

ABSTRACT: Tsunami is a catastrophic event that affects coastlines on a large scale with heavy casualties. Recent tsunami deposits and processes are studied for a better understanding of the disastrous event to enhance hazard assessment of tsunami-prone coastal areas. This research paper explores the 2004 tsunami deposits at Meulaboh (Aceh) to identify the thickness of post- and pre-tsunami deposits to improve risk assessment. The study consists of 4 Ground Penetrating Radar (GPR) survey lines near the Meulaboh shore. Two pit holes were dug along the survey lines and the deposition sequences were recorded. Records of the pit holes show good correlations with the intensity changes of EM waves from the GPR profiles and provide a clear insight into the subsurface tsunami deposit sequences at Meulaboh coastal area. The GPR results show that the 2004 pre-tsunami sediment deposits can be identified with a thickness of 0.3-1.5 m, while post-tsunami 2004 sediment deposits were also identified with a thickness of 0.1-1.2 m. Both sediment deposits known as alluvium were caused by natural coastal processes and erosion with an estimated depositional rate of 0.007-0.09 m/year. The thickness of the 2004 tsunami sediment deposits was identified as 0.2-3 m. This study revealed that the thickness of all the sediment deposits is thicker when approaching the shore, and GPR is a very efficient technique in investigating shallow subsurface with high data resolution to distinguish different deposits with high accuracy.

Keywords: GPR, Distinguishing, Tsunami Deposit, Post-Tsunami, Pre-Tsunami

1. INTRODUCTION

A good understanding of post-tsunami events which include the earthquake's magnitude, frequency, and history is needed to predict future tsunamis. Such information is crucial for coastal development, emergency facilities location,n and tsunami evacuation planning [1]. Especially in Aceh Province which experiences severe tsunamis. It is considered that the research regarding the tsunami deposits sediment is necessary to be carried out since the tsunami deposits caused by the large scale tsunami is rarely occurred and the research was also limited [2]. One of the post-tsunami studies that are often neglected is tsunami deposit. A tsunami deposit is sheets of soil deposits left after a tsunami event, preserved to form a geological sequence that acts as a record for scientists to understand past events and plays a significant role in future tsunami risk assessment. Data provided by geotechnical methods are accurate but costly and time-consuming, while geophysical data are less accurate compared to geotechnical data but are fast and inexpensive. Integration of geotechnical and geophysical data provides a suitable solution [3].

Boreholes or trial pits are geotechnical methods that are most common and widely applied by taking disturbed and undisturbed samples as well as conducting field tests (SPT, CPT, VST, etc.) including laboratory tests in determining specific gravity, Atterberg limits, moisture content, particle size analysis, permeability, etc. [4]. Despite the positive characteristics of geophysical methods, they have limitations that make the results obtained less accurate than those from geotechnical methods. Since the interpretation of geophysical data is much more complicated, it requires verification by geological and geotechnical data to provide an ideal approach to the subsurface survey [5, 6, 7, 8, 9].

The distribution of tsunami deposits near the shore is evidence of tsunami flooding which could be of use in estimating the relative magnitude of near and far tsunamis due to earthquakes [10]. Tsunami deposits are physically similar worldwide thus they could be a potential indicator for tsunami occurrence [11]. Tsunamis and their carried material cause many coastal environmental problems such as increasing the area of salt-water intrusion and disrupting the local hydrology and water quality. The collected information on tsunami

deposits is convenient for the government and public sectors to form an effective emergency management plan since the coastal population is gaining in numbers. Studies on coastal zone using satellite images, ground surveys, and sediment analyses have been well documented [12, 13], but very few studies on coastal change and tsunami deposits have been conducted for coastal planners to allocate resources and design appropriate structures for future hazards mitigation. Partial or complete rebuilding of sandy beaches after a hazard occurs takes a few months/years depending on inherited hydrologic and sedimentary parameters [14, 15, 16, 17]. This paper explores the 2004 tsunami that hit the western coast of Sumatra (Meulaboh, Aceh) to identify and characterize the tsunami deposits for a better understanding of their hazards locally and globally. Ground Penetrating Radar (GPR) was conducted to study the post-tsunami deposits and deposition rate. The results were validated with pit holes located near the GPR study lines.

2. MATERIALS AND METHODS

Sumatra Island is composed of metamorphic basement formation which has been intruded by plutonic formations and is overlaid by Mesozoic, Cenozoic, recent volcanic formations, and quaternary deposits (Fig. 1). Oldest rocks such as gneiss, schist, and quartzite are suspected to belong to several geological periods, folded and denuded before the deposition of Carboniferous beds. Sumatra Island's backbone is identified to be of these rock types as seen from outcrops and has been penetrated by Pre-Carboniferous granitic rock at several locations. Underlying these rocks are slates and limestone which are overlying older rocks of Upper Carboniferous age with some folding and could only be found in northern Sumatra. No Permian and Mesozoic deposits were found on the top part of the Kwalu basin of East Sumatra. Tertiary deposits (low layer regions) are widely spread over the plains and consist of breccias, conglomerates, sandstones, marls, and limestones, with seams of coal and lignite. Coal was identified in Eocene beds with eruptions of augite-andesite occurring along the west coast. Miocene formation mainly consists of margins and occasional lignite and limestone embedded with occasional petroleum. Pliocene formation (low-lying land) overlies alluvium which is composed of seams of lignite and brown coal [18].

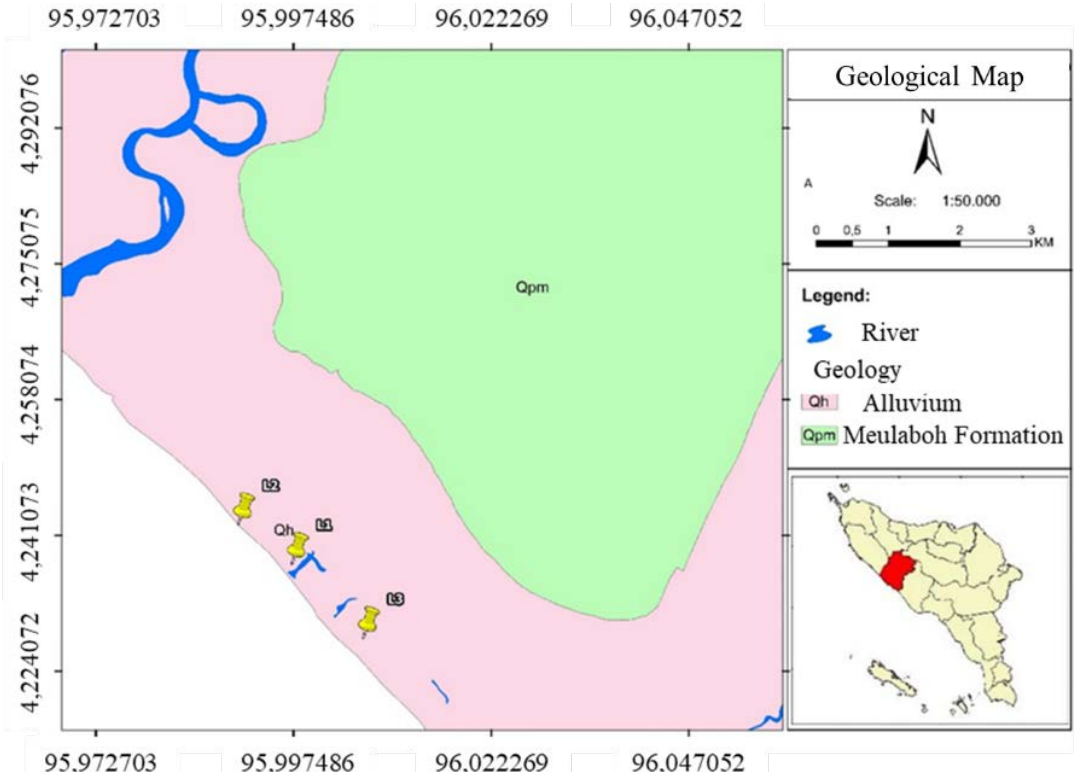

Fig. 1 Geology of Sumatra Island (modified from [19], [20])

The study was conducted along the coastal line of Meulaboh (Aceh), the western shore of Sumatra Island using the MALA GPR system with a 250 MHz shielded antenna. The system applied 5599 MHz sampling frequency; 1224 sampling numbers; 2 stacking numbers; 219 ns time window and 0.023

m trace interval. The GPR method works based on the principle of reflection and refraction concepts of EM waves. Two GPR survey lines were conducted in the Suak Pante Breuh area (A and B) and one line in the Suak Seukee area (C) (Fig. 2). The location of the survey lines was selected with consideration of the coastline pattern along the stretch of the coast impacted by the tsunami.

EM waves of GPR were recorded along a survey line by stacking each wave trace laterally such that low-intensity signals represent homogenous sediments whereas an increase in intensity is associated with greater contrast between inter-sediments characteristics. Changes in electromagnetic and dielectric properties of tsunami deposits are ideal for producing better GPR images since the high conductivity of the deposits changes the flow of electrical current. EM properties in the subsurface material are estimated using Maxwell's equation where their behavior is dependent on the electrical conductivity and dielectric constant, □r of the subsurface and are expressed in Equations 1 and 2 [21].

$$\Delta X E = -jw\mu H \quad (1)$$

$$\Delta X H = E\sigma + w\varepsilon E \quad (2)$$

Where E is electric field intensity, H is magnetic field intensity, j is electric current density, μ is magnetic permeability, and σ is dielectric conductivity and dielectric permittivity.

The velocity of the wavelet is dependent on the material's dielectric properties (Equation 3), while the reflected signal is given by Equation 4 and the refraction signal by Snell's law shown in Equation 5 [22].

$$v = \frac{c}{\sqrt{\varepsilon_r}} \quad (3)$$

$$R = \left(\sqrt{\varepsilon_2} - \sqrt{\varepsilon_1}\right)/\left(\sqrt{\varepsilon_2} + \sqrt{\varepsilon_1}\right) \quad (4)$$

$$\frac{\sin \alpha_1}{v_1} = \frac{\sin \alpha_2}{v_2} \quad (5)$$

where *v* is the velocity in medium, c is the speed of light in vacuum and α_1 and α_2 are the attenuation coefficients of the material.

The total length of the survey line at survey area A is 368.28 m and the line was divided into two sub-lines: L1a and L1b with total lengths of 152.62 m and 215.66 m, respectively. Survey line L2 located at survey area B is 182.12 m long and L3 at survey area C is 118.09 m long. Two pit holes; P1 and P2 were dug for correlation and interpretation purposes (Fig. 3). P1 is located at a distance of 46 m on line L1b and P2 is located on line L3 at a distance of 14 m (Fig. 2). All GPR surveys were conducted starting from the shoreline towards the inland with a bearing of 45o N. The GPR data was processed using Reflex-W version 5.0 to identify the velocity and depth of the subsurface for each survey line. Values obtained from the lines were correlated with their respective pit holes (line L1b with pit P1 and line L3 with pit P2) to validate the velocity and depth values for soil type classification. These values were converted to Microsoft Excel format and subsurface models were plotted using Surfer 8 software for interpretation.

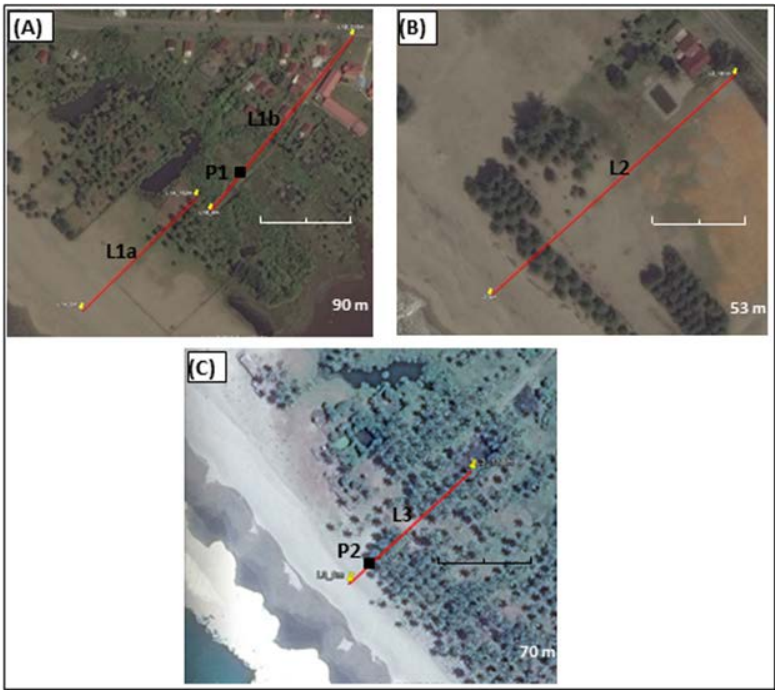

Fig. 2 GPR survey lines at Meulaboh, Aceh; (A and B) Suak Pante Breuh area, (C) Suak Seukee area. P1 and P2 pits are located at lines L1b and L3 respectively [23]

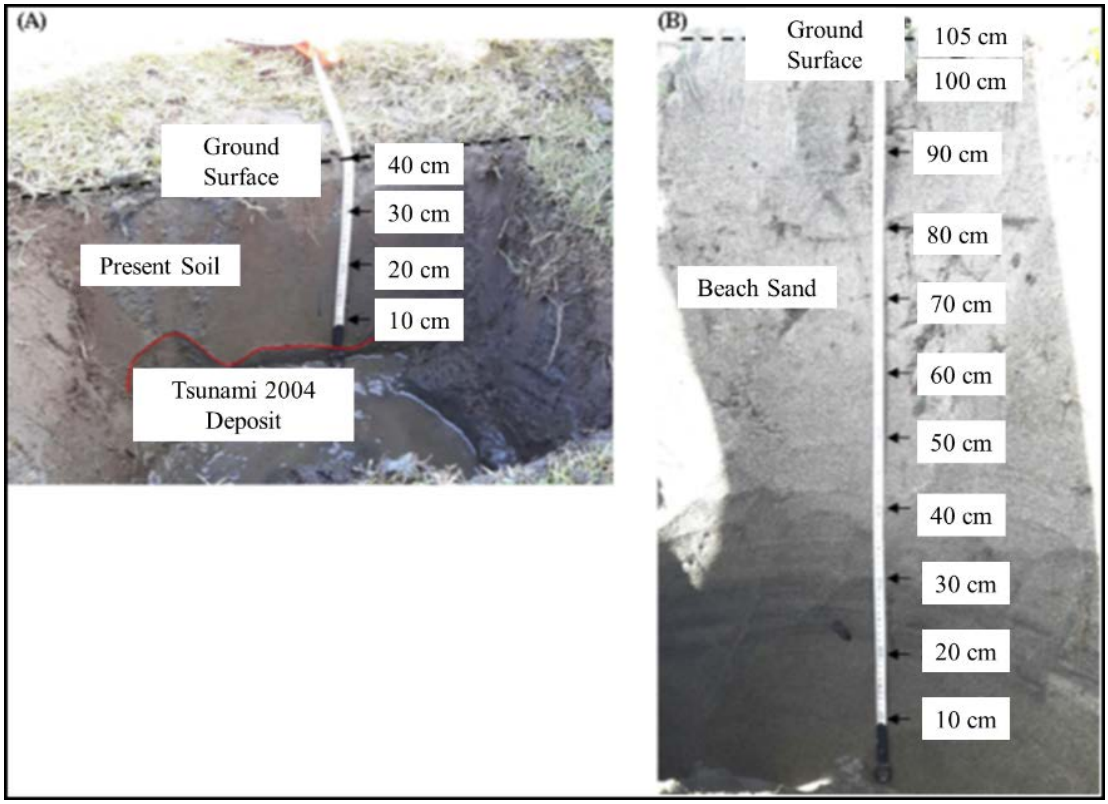

Fig 3. Pit holes at Meulaboh; (A) P1 at 46 m on line L1b and (B) P2 at 14 m on line L3

3. DATA AND RESULTS

Fig.4-7 shows the processed data of lines L1a, L1b, L2, and L3, respectively. The reflection of the EM wave can be seen within a depth of 0-5 m. Line L1a and L1b consist of four subsurface soil layers with a thickness of less than 2.5 m for all layers, while lines L2 and L3 consist of three soil subsurface layers with a thickness of less than 1.5 m. The variation in EM waveform detects changes that occur at stratigraphic boundaries, as the higher intensity of waves merges to form strong reflection surfaces. It also detects less drastic changes within the layers that have lower EM wave intensity to form medium to weak reflections. The GPR results show the boundary between existing soil (alluvium), tsunami deposits, and present silty deposits as horizontal homogeneous reflectors as the upper silt layer, followed by the boundary to underlying tsunami deposits marked by a strong continuous reflection whereas the third layer is distinguished by higher wave attenuation. The pit holes show varying characteristics of the pre-and post-tsunami deposits which are clearly illustrated by the deposit's distribution, either naturally (caused by climate cycles) or forced during an extreme event (Fig. 3). The difference in grain size and colors of deposits indicate a clear distinction between different layers. Finer grain size and bright-colored deposits represent 2004 pre-tsunami deposits while medium grain size, dark-colored deposits, and poorly sorted and swarthy sediments represent 2004 tsunami deposits. The post-2004 tsunami deposits have medium to coarser grain size deposits. The existing research regarding the post-tsunami sediment deposits in Aceh province carried out by implementing resistivity and chargeability data also showed the same pattern [24].

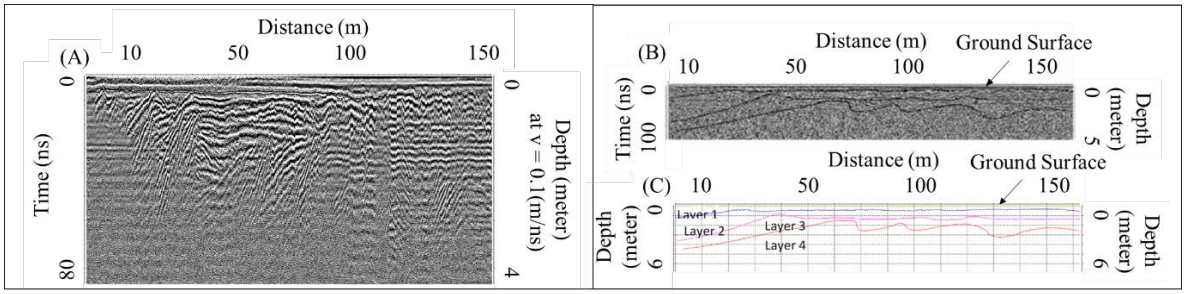

Fig. 4 GPR data of line L1a; (a) processed data, (b) interpreted data, and (c) subsurface boundary.

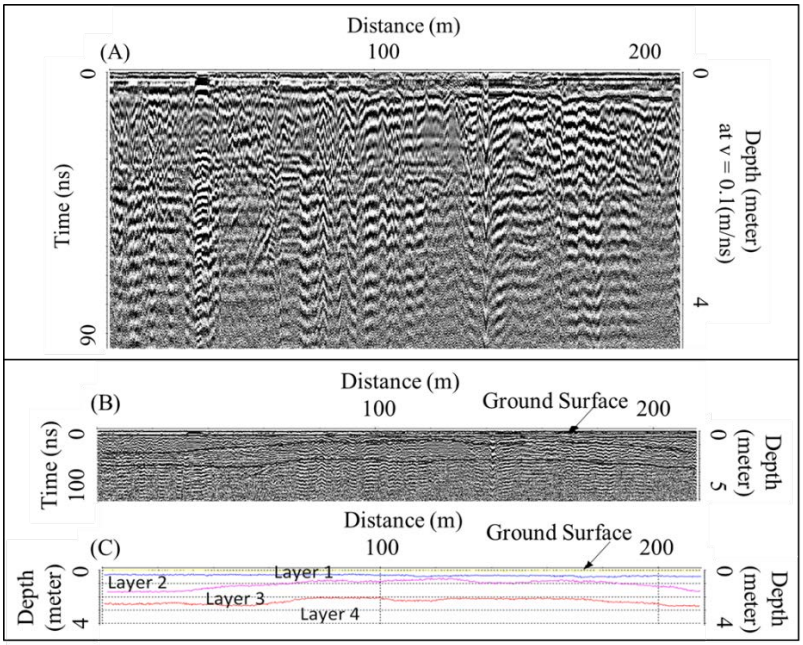

Fig. 5 GPR data of line L1b; (a) processed data, (b) interpreted data, and (c) subsurface boundary.

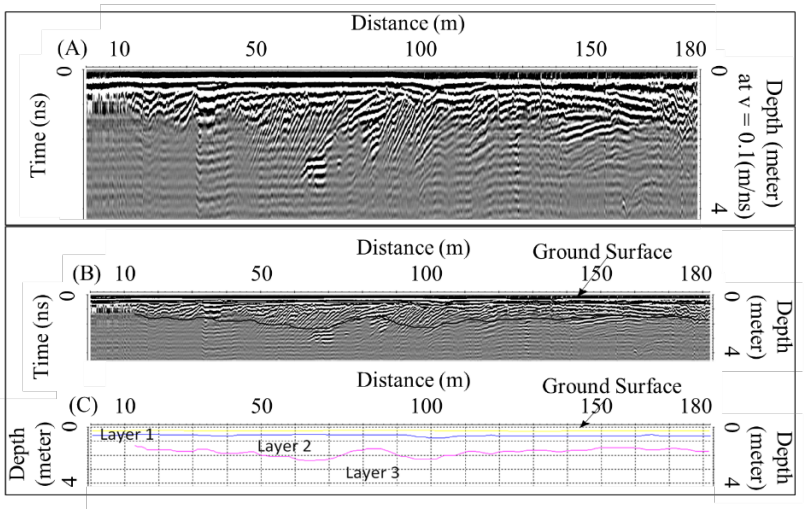

Fig. 6 GPR data of line L2; (a) processed data, (b) interpreted data, and (c) subsurface boundary.

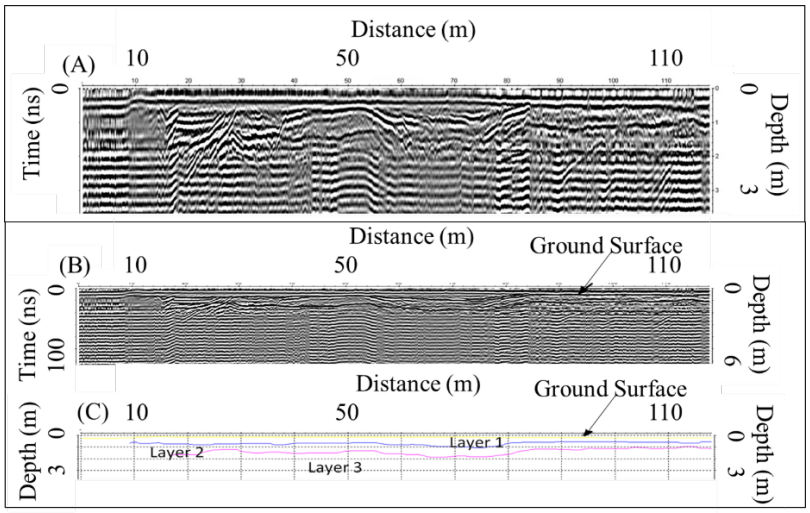

Fig. 7 GPR data of line L3; (a) processed data, (b) interpreted data, and (c) subsurface boundary.

4. DISCUSSION

The GPR results were correlated with pit holes for validation and to identify the different deposits along the survey lines that underwent erosional/depositional processes (top-soil) due to extreme events which are common along the west coast of Aceh. The coarser and darker deposits of the lower layer were interpreted as tsunami deposits from the GPR results where the layer is situated beneath the second reflector line. Fig. 8 shows all the GPR results plotted according to elevation versus distance using an x:z scale ratio of 1:10 for lines L1a, L1b, and L2, and 1:8 for the liner to identify the variation of the subsurface deposits.

Lines L1a and L1b (Fig. 8a and 8b) show that the top layer was deposited after the 2004 tsunami (post-tsunami) with a thickness of 0.3-1.2 m while the second layer is the 2004 tsunami deposit with a thickness of 0.2-3 m. The third and fourth layers are alluvium before the 2004 tsunami (pre-tsunami) with a thickness of 0.3-1.5 m and a depth of 2-3 m. Lines L2 and L3 (Fig. 8c and 8d) also show similar results where the first layer is a post- 2004 tsunami deposit with a thickness of 0.1-1.2 m; followed by a 2004 tsunami deposit with a thickness of 0.2-2 m and lastly, an alluvium layer that was deposited pre-2004 tsunami with the thickness of 0.3-1.5 m and depth of 1.5-3 m for each line respectively.

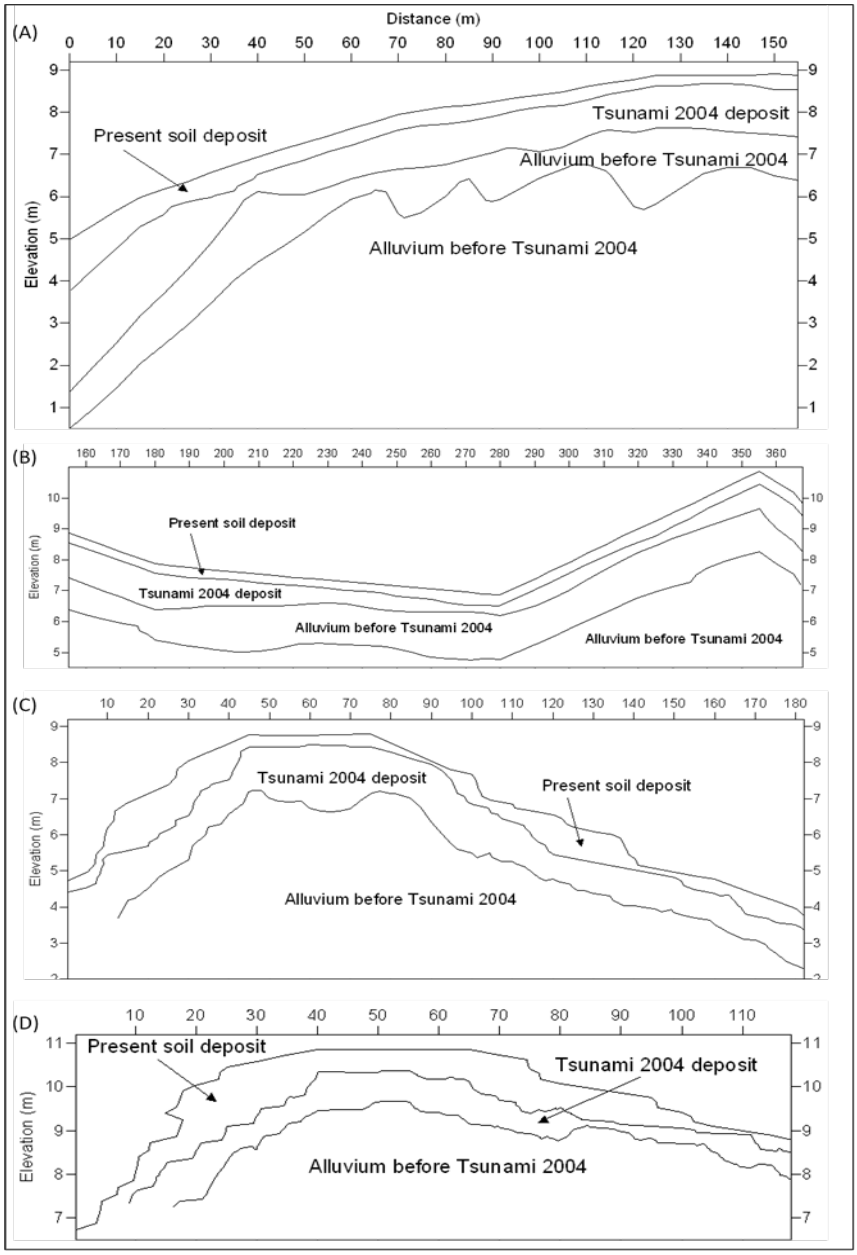

Fig. 8 The schematic representation of the GPR image shows the ing soil subsurface plot of all GPR study lines; (a) Line L1a with scale ratio x:z of 1:10, (b) Line L1b with scale ratio x:z of 1:10, (c) Line L2 with scale ratio x:z of 1:10 and (d) Line L3 with scale ratio x:z of 1:

5. CONCLUSION

The sediment in the Meulaboh district has been distinguished into three types: pre-tsunami, tsunami, and post-tsunami. The 2004 pre-tsunami sediment deposits known as alluvium are caused by natural coastal processes and erosion, identified with a thickness of 0.3-1.5 m. The 2004 post-tsunami sediment deposits (alluvium) are identified with a thickness of 0.1-1.2 m which are also caused by the same process as pre-tsunami 2004. The depositional rate of both sediment deposits is estimated to be 0.007-0.09 m/year. Tsunami sediment deposits caused by extreme events (tsunami 2004) have a thickness of 0.2-3 m. Generally, the thickness of each layer increases when approaching the shore. The deposition layers detected from the pit holes show a good correlation with GPR data. Strong correlations between GPR profiles and pit holes show that GPR is a very efficient technique in investigating shallow subsurfaces with high data resolution to distinguish different deposit layers with high accuracy**.**

6. ACKNOWLEDGEMENT

Many thanks to the Ministry of Education, Culture, Research, and Technology, Indonesia for the financial support for fieldwork in the scheme of the Competitive Research Grant, as well as the Science and Technology Center of Excellent (PUI) TDMRC-USK Program (2018), and PP No.024/UN.11.2.1/PT.01.03/PNBP/2022 Research Grant for preparing, editing, and publishing the article. Special thanks are extended to the technical staff of Geophysics Laboratory and Geophysics Postgraduate Students, Universiti Sains Malaysia and Physics dan Geophysics Students, Faculty of Sciences and Faculty of Engineering, Syiah Kuala University.

7. REFERENCES

[1] Geist, Eric L., Helping Coastal Communities at Risk from Tsunamis--the Role of US Geological Survey Research, US Department of the Interior, US Geological Survey Vol. 150, 2000.

[2] Syukri, M., Anda, S. T., Safitri, R., Fadhli, Z., & Saad, R., Prediction of Soil Liquefaction Phenomenon in Banda Aceh and Aceh Besar, Indonesia Using Electrical Resistivity Tomography (ERT), International Journal of GEOMATE, Vol. 18, Issue 70, 2020, pp. 123-129.

[3] Rezaei, S., Shooshpasha, I. & Rezaei, H., Empirical Correlation between Geotechnical and Geophysical Parameters in a Landslide Zone (Case Study: Naigeschal Landslide), Earth Sciences Research Journal, Vol. 22, Issue 3, 2018, pp. 195-204.

[4] Gui-Sheng, H., Ning-Sheng, C., Javed Iqbal, T., Yong, Y., & Jun, L., Case study of the characteristics and dynamic process of July 10, 2013, catastrophic debris flows in Wenchuan County, China. Earth Sciences Research Journal, Vol. 20, Issue 2, 2016, pp. 1-13.

[5] Ozcep, F., Tezel, O., & Asci, M., Correlation between electrical resistivity and soil-water content: Istanbul and Golcuk, International Journal of Physical Sciences, Vol. 4, Issue 6, 2009, pp. 362-365.

[6] Osman, S., Baharom, S., & Siddiqui, F. I., Correlation of electrical resistivity with some soil parameters for the development of possible prediction of slope stability and bearing capacity of soil using electrical parameters, Pertanika Journal Science and Technology, Vol. 22, Issue 1, 2014, pp. 139-152.

[7] Sil, A., & Haloi, J., Empirical correlations with standard penetration test (SPT)-N for estimating shear wave velocity applicable to any region, International Journal of Geosynthetics and Ground Engineering, 3(3), 2017, pp. 22.

[8] Thokchom, S., Rastogi, B. K., Dogra, N. N., Pancholi, V., Sairam, B., Bhattacharya, F., & Patel, V., Empirical correlation of SPT blow counts versus shear wave velocity for different types of soils in Dholera, western India, Natural Hazards, Vol. 86, Issue 3, 2017, pp. 1291-1306.

[9] Jusoh, H., & Osman, S. B. S., The correlation between resistivity and soil properties as an alternative to soil investigation, Indian Journal of Science and Technology, Vol. 10, Issue 6, 2017.

[10] Jaffe, B. E, and Gelfenbaum, G., Using tsunami deposits to improve assessment of tsunami risk, Solutions to Coastal Disasters ‘02, Conference Proceedings ASCE, 2002, pp. 836-847.

[11] Peters, R., Jaffe, B., Gelfenbaum, G. and Peterson, C., Cascadia Tsunami Deposit Database: U.S. Geological Survey Open-File Report 03–13, 2003.

[12] Fritz, H.M., Kongko, W., Moore, A., McAdoo, B., Goff, J., Harbitz, C., Uslu, B., Kalligeris, N., Suteja, D., Kalsum, K. and Titov, V., Extreme runup from the 17 July 2006 Java tsunami, Geophysical Research Letters 34, No. 12, 2007.

[13] Spencer, T., Brooks, S. M., Möller, I., & Evans, B. R., Where local matters: impacts of a major North Sea storm surge, Eos, Transactions American Geophysical Union, 95(30), 2014, pp. 269-270.

[14] Wang, P., Kirby, J. H., Haber, J. D., Horwitz, M. H., Knorr, P. O. & Krock, J. R., Morphological and sedimentological impacts

of Hurricane Ivan and immediate post-storm beach recovery along the Northwestern Florida Barrier-Island Coasts, Journal of Coastal Research 22, Vol. 6, Issue 226, 2006, pp. 1382-1402.

[15] Yu, F., Switzer, A.D., Lau, A.Y.A., Yeung, H.Y.E., Chik, S.W., Chiu, H.C., Huang, Z. and Pile, J., A comparison of the post-storm recovery of two sandy beaches on Hong Kong Island, southern China, Quaternary international, 2013, pp.163-175.

[16] Choowong, M., Phantuwongraj, S., Charoentitirat, T., Chutakositkanon, V., Yumuang, S., & Charusiri, P., Beach recovery after 2004 Indian Ocean tsunami from Phang-nga, Thailand, Geomorphology, Vol. 104, No. 3-4, 2009, pp. 134-142.

[17] Liew, S.C., Gupta, A., Wong, P.P. and Kwoh, L.K., Recovery from a large tsunami mapped over time: the Aceh coast, Sumatra, Geomorphology, Vol. 114, No. 4, 2010 pp.520-529.

[18] Bennett, J. D., McC Jeffrey, D., Bridge, D., Cameron, N. R., Djunuddin, A., Ghazali, S. A., Jeffrey, D. H., Kartawa, W., Keats, W., Rock, N. M. S., Thomson, S. J. & Whandoyo, R., Geologic map of the Banda Aceh Quadrangle, Sumatra, 1981.

[19] Stephenson, B., and J. A. Aspden. Simplified geological map of Northern Sumatra. Directorate of Overseas Surveys, Keyworth, 1982.

[20] S. Gafoer, T.C. Amin, R. Pardede, Geological Map of Indonesia, Geological Research and Development Centre, Bandung, Indonesia, 1992.

[21] Alsharahi, G., Driouach, A. and Faize, A., Performance of GPR influenced by electrical conductivity and dielectric constant, Procedia Technology, Vol. 22, 2016, pp.570-575.

[22] David, D., Ground-penetrating radar. The Institution of Electrical Engineers, London, United Kingdom, 2nd Ed, 2004.

[23] Google Earth, 2016

[24] Syukri, M., Saad, R., Anda, S. T., & Fadhli, Z. Resistivity and Chargeability Signatures of Tsunami Deposits at Aceh Besar and Banda Aceh Coastal Area, Indonesia. International Journal, Vol 17, No. 59, 2019, 133-143.